

ARTICLE OPEN



MLKL deficiency protects against low-grade, sterile inflammation in aged mice

Emma C. Tovey Crutchfield^{1,2,3,5}, Sarah E. Garnish^{1,2,5}, Jessica Day^{1,2,4}, Holly Anderton^{1,2}, Shene Chiou^{1,2}, Anne Hempel¹, Cathrine Hall¹, Komal M. Patel¹, Pradnya Gangatirkar¹, Katherine R. Martin^{1,2}, Connie S. N. Li Wai Suen¹, Alexandra L. Garnham¹, Andrew J. Kueh^{1,2}, Ian P. Wicks^{1,2,4}, John Silke^{1,2}, Ueli Nachbur^{1,2}, Andre L. Samson^{1,2}, James M. Murphy^{1,2,6} and Joanne M. Hildebrand^{1,2,6}

© The Author(s) 2023, corrected publication 2023

MLKL and RIPK3 are the core signaling proteins of the inflammatory cell death pathway, necroptosis, which is a known mediator and modifier of human disease. Necroptosis has been implicated in the progression of disease in almost every physiological system and recent reports suggest a role for necroptosis in aging. Here, we present the first comprehensive analysis of age-related histopathological and immunological phenotypes in a cohort of *Mkl1*^{-/-} and *Ripk3*^{-/-} mice on a congenic C57BL/6 J genetic background. We show that genetic deletion of *Mkl1* in female mice interrupts immune system aging, specifically delaying the age-related reduction of circulating lymphocytes. Seventeen-month-old *Mkl1*^{-/-} female mice were also protected against age-related chronic sterile inflammation in connective tissue and skeletal muscle relative to wild-type littermate controls, exhibiting a reduced number of immune cell infiltrates in these sites and fewer regenerating myocytes. These observations implicate MLKL in age-related sterile inflammation, suggesting a possible application for long-term anti-necroptotic therapy in humans.

Cell Death & Differentiation (2023) 30:1059–1071; <https://doi.org/10.1038/s41418-023-01121-4>

INTRODUCTION

Necroptosis is a programmed form of lytic cell death that culminates in the rupture of biological membranes and subsequent release of inflammatory, intracellular constituents termed DAMPs (damage-associated molecular patterns) [1]. Necroptosis is triggered by a range of both host- and pathogen-derived stimuli, culminating in the phosphorylation of mixed lineage kinase domain-like (MLKL) by the receptor-interacting serine/threonine protein kinase 3 (RIPK3) [2–4]. Phosphorylated MLKL oligomerises and dissociates from RIPK3, before translocating to biological membranes where it accumulates and disrupts plasma membrane integrity [5–10].

In mice, the genetic deletion of *Mkl1* or *Ripk3* does not impose overt developmental or early-life homeostatic defects on mice [4, 11–14], except for some asymptomatic renovascular [15], neurovascular [16] and trabecular [17] differences reported in *Ripk3*-deficient mice generated on a C57BL/6N background. At 3 months of age, *Mkl1*^{-/-} and *Ripk3*^{-/-} mice are macroscopically indistinguishable and share similar peripheral blood cell and platelet populations to their wild-type littermates [4, 12–14, 18]. Yet, in response to challenge, *Mkl1*^{-/-} and *Ripk3*^{-/-} mice often respond differently to their wild-type counterparts, and each other. This has been demonstrated in models of *Staphylococcus aureus* infection [19, 20], renal ischemia-reperfusion injury [16, 21], dermatitis [22, 23] and others (recently reviewed in ref. [24]).

Differences between *Mkl1*^{-/-} and *Ripk3*^{-/-} mice have been attributed to the necroptosis-independent roles of MLKL and RIPK3, for example in NF-κB activation, inflammasome activation, apoptosis signaling, and endosome/exosome formation [25–30]. It is important to note, however, that comparisons between *Mkl1*^{-/-} and *Ripk3*^{-/-} mice are not always performed in parallel and therefore interfacility variability in housing conditions and ambient microbiomes are likely to contribute to divergent phenotypes between studies. Additionally, the most commonly used *Mkl1*^{-/-} mouse lines were generated and are maintained on a C57BL/6 J background [4, 12], while the most used *Ripk3*^{-/-} mouse line is C57BL/6NJ [14]. Despite being derived from the same original mouse strain, 6 J and 6NJ are separated by over 60 years of independent breeding and demonstrate profound differences in morbidity and mortality following inflammatory challenges, for example, in LPS- or TNFα-induced sepsis [31] and Influenza A virus infection [32].

The absence of *Mkl1* and *Ripk3* has been variably reported to influence aging of the male reproductive system in mice. Male *Mkl1*^{-/-} and *Ripk3*^{-/-} mice were shown to exhibit youthful seminiferous tubules and extended reproductive longevity relative to wild-type males of the same age in an initial study [11]. These findings were challenged in a subsequent study that reported no evidence for genotype-dependent testicular aging [33].

As a result of the high prevalence of dysregulated necroptosis in a vast range of human disease [21, 34–41], the therapeutic

¹The Walter and Eliza Hall Institute, Parkville, VIC, Australia. ²The University of Melbourne, Department of Medical Biology, Parkville, VIC, Australia. ³The University of Melbourne, Faculty of Medicine, Dentistry and Health Sciences, Parkville, VIC, Australia. ⁴Royal Melbourne Hospital, Rheumatology Unit, Parkville, VIC, Australia. ⁵These authors contributed equally: Emma C. Tovey Crutchfield, Sarah E. Garnish. ⁶These authors jointly supervised this work: James M. Murphy, Joanne M. Hildebrand. ✉email: jamesm@wehi.edu.au; jhildebrand@wehi.edu.au

Received: 12 October 2022 Revised: 16 January 2023 Accepted: 23 January 2023

Published online: 8 February 2023

targeting of the necroptotic pathway is being actively pursued on several fronts. While upstream serine/threonine kinase, RIPK1, has been the target of many clinical trials for autoimmune conditions (e.g., rheumatoid arthritis [42]), neurodegeneration (e.g., amyotrophic lateral sclerosis [43]) and cancer (e.g., pancreatic ductal adenocarcinoma [44]), no MLKL- or RIPK3-binding compounds have been included in human trials to date. In light of three recent clinical reports linking *MLKL* loss-of-function mutations to neurodegeneration [45, 46] and diabetes [47], modeling the impact of prolonged MLKL loss in mice is integral to understand if therapeutic inhibition of MLKL could contribute to the development or progression of human disease.

Accordingly, here we present a comprehensive characterization of aged *Mkl1*^{-/-} and *Ripk3*^{-/-} mice relative to wild-type littermate controls. Both strains have been bred, housed, and examined in the same facility under identical conditions, and the *Ripk3*^{-/-} knockout strain, published for the first time here, was generated on the C57BL/6J background. These studies have identified a novel role for MLKL in aging, revealing a delay in the age-related reduction in circulating lymphocytes and a protection from chronic, low-grade, sterile inflammation in female *Mkl1*^{-/-} aged mice.

RESULTS

Generation of *Ripk3*^{-/-} mice on a C57BL/6J background

To permit direct comparison with the previously generated *Mkl1*^{-/-} C57BL/6J strain [4], we developed a new *Ripk3*^{-/-} strain on a C57BL/6J genetic background via CRISPR-Cas9 mediated disruption of the mouse *Ripk3* locus (Supplementary Fig. 1A). Mice were born according to expected Mendelian ratios and showed no overt signs of disease (Supplementary Fig. 1B), consistent with the previously described *Ripk3*^{-/-} strain generated using homologous recombination on a C57BL/6NJ background [14]. Immunoblots of protein extracts from a range of organs demonstrated that RIPK3 was readily detectable in all examined organs in wild-type mice but was absent in tissues of *Ripk3*^{-/-} mice, verifying deletion of the *Ripk3* protein product (Supplementary Fig. 1C). Immortalised mouse dermal fibroblasts (MDFs) isolated from wild-type and *Ripk3*^{-/-} mice were examined for their sensitivity to death stimuli. As expected, *Ripk3*^{-/-} MDFs did not die in response to TSI-induced (TNF; Smac-mimetic, Compound A; pan-caspase inhibitor, IDN-6556; termed TSI) necroptosis, with the hallmark of the necroptosis pathway activation—the phosphorylation at Serine 345 within mouse MLK3 [4]—not observed (Supplementary Fig. 1D, E). In response to TNF and Smac-mimetic-induced apoptosis, *Ripk3*^{-/-} MDFs exhibited reduced levels and kinetics of death in comparison to wild-type MDFs (Supplementary Fig. 1D). These data validate successful RIPK3 deletion in a mouse strain of C57BL/6J background, which can be used as a tool to compare phenotypic differences between otherwise congenic *Mkl1*^{-/-} and *Ripk3*^{-/-} mouse strains.

Mkl1^{-/-} and *Ripk3*^{-/-} mice show no overt differences in male reproductive system aging

To determine the long-term consequences resulting from necroptotic signaling deficiency, a cohort of wild-type, littermate-controlled, *Mkl1*^{-/-} and *Ripk3*^{-/-} mice were aged to 12 months. As observed previously, 12-month-old *Mkl1*^{-/-} and *Ripk3*^{-/-} mice displayed no overt disease or change in rates of mortality [11, 13, 33]. In contrast to previous reports [11, 15], body weights of male *Mkl1*^{-/-} mice, and male and female *Ripk3*^{-/-} mice were, on average, equivalent to wild-type littermate controls (Fig. 1A). Female *Mkl1*^{-/-} mice were, however, on average, 12% heavier than wild-type littermate controls (Fig. 1A). This increase in body weight was not driven by differences in the weight of any one specific organ we measured (Fig. 1B, Supplementary Fig. 1F–H). The weights of all organs were comparable between *Mkl1*^{-/-} or *Ripk3*^{-/-}

and their respective wild-type littermate controls with the exception of the spleen in *Ripk3*^{-/-} males (Fig. 1B–D, Supplementary Fig. 1F–H). When presented as a percentage of body weight, *Ripk3*^{-/-} males had a 12% decrease in relative spleen weight compared to wild-type littermate controls, however the splenic architecture remained intact and no macroscopic pathologies were observed (Fig. 1B, E). In support of recent observations [33], 12-month-old *Mkl1*^{-/-} and *Ripk3*^{-/-} males had on average, equivalent seminal vesicle and testes weights compared to their respective wild-type littermate controls (Fig. 1C, D). Overall, the absence of *Mkl1* and *Ripk3* at 12 months of age did not result in any overt phenotypic differences in the major reproductive and non-reproductive organs.

Mkl1^{-/-} mice do not develop overt neurodegenerative or diabetic disease at 9 months of age

In response to three recent clinical reports of human *MLKL* loss-of-function mutations associated with severe neurological or diabetic disease [45–47], aged mice deficient in *Mkl1* or *Ripk3* were assessed for signs of these conditions. The patients identified in these reports presented with disease onset as late as 30 years of age, therefore mice were aged to 9 months which roughly equates to 35 human years [48]. These mice were examined by professional histopathologists, blinded to genotype. All mice, irrespective of genotype, were classified as ostensibly normal and displayed intact gross motor and neurological function as measured by gait and the tail suspension test [49] (Supplementary Fig. 2A, Supplementary File 1). None of the characterised neurodegenerative lesions present in male human carriers of homozygous *MLKL* loss-of-function mutation, *p.Asp369GlufsTer22* (rs56189347) were observed in brain sections of *Mkl1*^{-/-} and wild-type littermate control mice [46] (Fig. 2A, Supplementary Fig. 2B). There was no evidence of global atrophy or periventricular white matter lesions observed in H&E-stained brain sections, and full body X-rays showed no evidence of osteoporosis, such as bone thinning or fractures, which are common comorbidities associated with neurological disorders [50] (Fig. 2A, B, Supplementary Fig. 2B, C, Supplementary File 1). All brains were symmetrical and similar in size, measured by length, width, and height (Supplementary Fig. 2D). A rare missense loss-of-function mutation in *MLKL* was also found to exclusively segregate with the affected male and female siblings suffering from maturity-onset diabetes of the young (MODY) [47]. Random blood glucose measurements taken from *Mkl1*^{-/-} and *Ripk3*^{-/-} mice at 6 and 12 months revealed no pre-diabetic or diabetic phenotypes. At both 6 and 12 months of age, *Mkl1*^{-/-} and *Ripk3*^{-/-} mice had random blood glucose measurements equivalent to littermate controls (Fig. 2C, D). Further, H&E-stained pancreas sections of 9-month-old mice revealed no lesions of significance, with typical exocrine and endocrine tissue architecture (Fig. 2E, F).

Mkl1^{-/-} mice exhibit age-dependent increases in peripheral lymphocyte numbers

Extending the phenotyping of our aged *Mkl1*- and *Ripk3*-deficient cohort, peripheral blood cell numbers were quantified in *Mkl1*^{-/-} and *Ripk3*^{-/-} mice from 3 to 14 months. Fourteen-month-old male and 12-month-old female *Mkl1*^{-/-} mice displayed, respectively, a 57% and 44% increase in the average number of peripheral white blood cells (WBC) compared to their wild-type littermate controls (Fig. 3A). This change in WBC number was driven by increases in the peripheral lymphocyte population. In comparison to wild-type littermate controls, peripheral lymphocytes were elevated by 61% in 14-month-old male *Mkl1*^{-/-} mice and by 51% in 12-month-old female *Mkl1*^{-/-} mice (Fig. 3B). Three-month-old male and female *Mkl1*^{-/-} mice also displayed, respectively, a 60% and 48% increase in the average number of peripheral neutrophils compared to wild-type littermate controls (Fig. 3C). This increase in peripheral neutrophils was accompanied by a 50% increase in the average

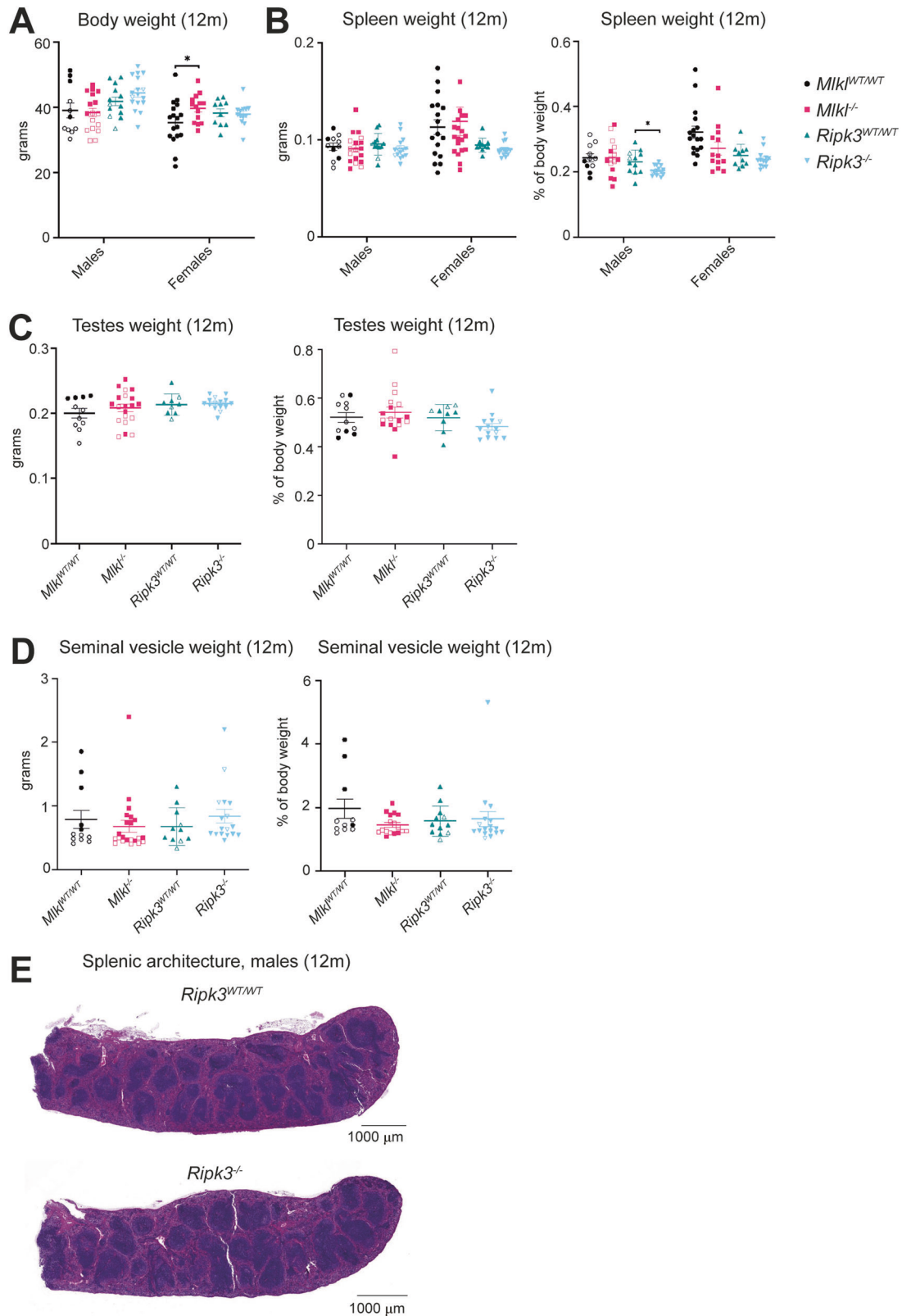
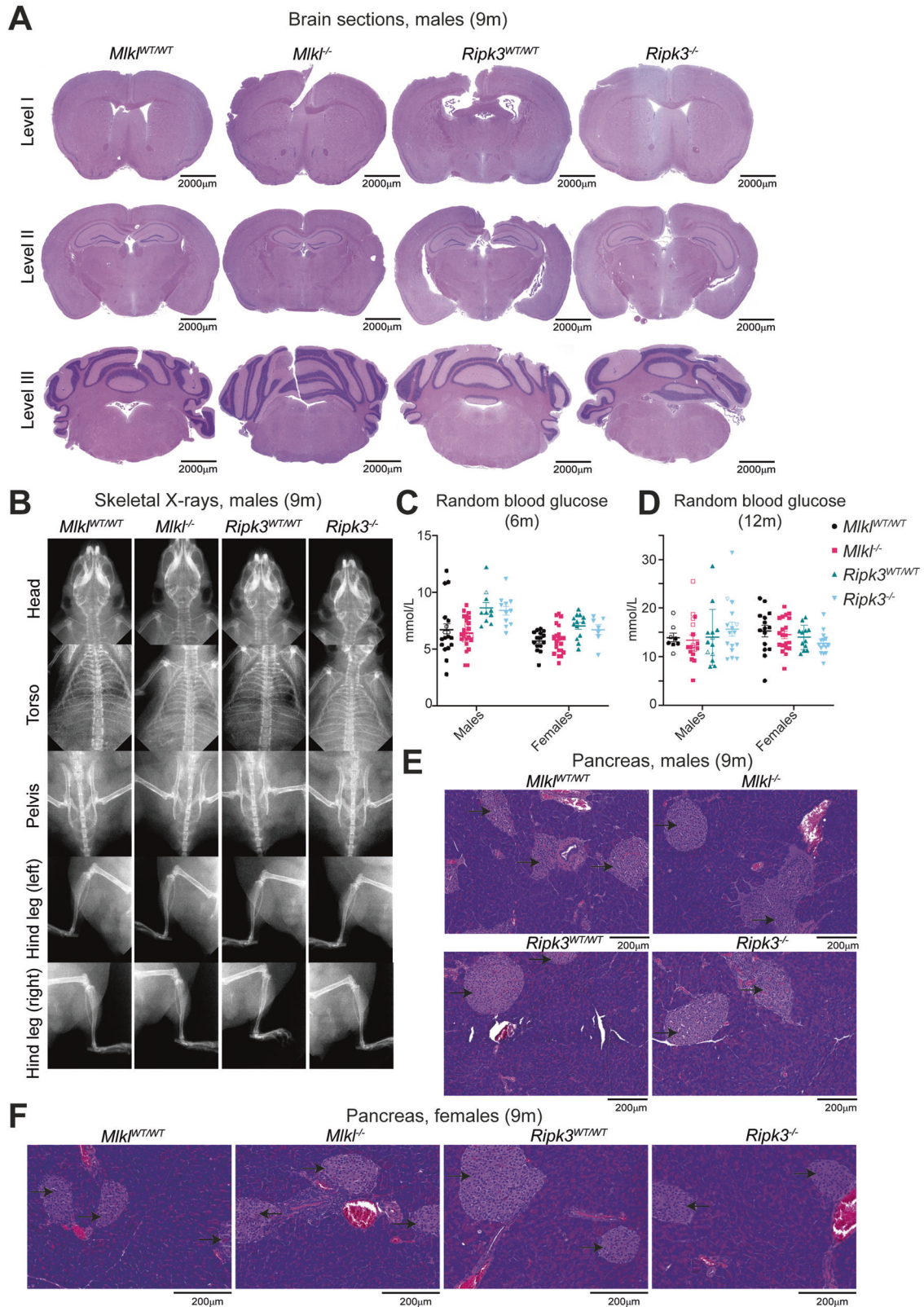


Fig. 1 *Ripk3^{-/-}* male mice exhibit reduced spleen weight in comparison to wild-type littermate controls. **A** Body weights of *Mik1^{-/-}*, *Ripk3^{-/-}* and wild-type littermate control mice at 12 months of age. Weight (absolute and relative) of 12-month-old *Mik1^{-/-}*, *Ripk3^{-/-}* and wild-type littermate control spleen (**B**), testes (**C**) and seminal vesicles (**D**). **E** H&E-stained section of male *Ripk3^{-/-}* mice and wild-type littermate control at 12 months of age. Each symbol represents a datum from one individual mouse and error bars represent mean \pm SEM for $n = 9-20$. Hollowed-out symbols represent data from fighting male mice. H&E-stained sections of the spleen (**E**) are representative of $n = 7-9$ mice per genotype. * $p < 0.05$ was calculated using an unpaired, two-tailed Student's *t* test.



number of peripheral monocytes in 3-month-old female *Mik1*^{-/-} mice compared to wild-type littermate controls (Fig. 4D). Despite these significant variations in white blood cell counts, bone marrow and peripheral blood smears from 9- and 17-month-old *Mik1*^{-/-} mice demonstrate morphologically indistinguishable

lymphoid and myeloid cells to wild-type littermate controls (Supplementary File 1). Female, but not male, *Ripk3*^{-/-} mice also exhibited significant differences in their peripheral WBC populations across age (Fig. 3A–E). A 24% reduction in the mean circulating WBC population was observed in female *Ripk3*^{-/-} mice

Fig. 2 No overt macroscopic signs of neurodegenerative or diabetic disease were observed in 9-month-old *Mik1*^{-/-} and *Ripk3*^{-/-} mice. **A** H&E-stained sections of the levels I, II and III of the brain and **(B)** X-ray images of the head, torso, pelvis, and hind leg from 9-month-old male *Mik1*^{-/-}, *Ripk3*^{-/-} and wild-type littermate control mice. Level I includes the cortex, corpus callosum, caudate putamen and lateral ventricles; level II includes the hippocampus, thalamus, hypothalamus, and lateral and third ventricles, and level III, the cerebellum, pons and fourth ventricle. Random blood glucose measurements for 6- **(C)** and 12-month-old **(D)** *Mik1*^{-/-}, *Ripk3*^{-/-} and wild-type littermate control mice. H&E-stained sections from the pancreas of 9-month-old male **(E)** and female **(F)** *Mik1*^{-/-}, *Ripk3*^{-/-} and wild-type littermate control mice. Islets of Langerhans are denoted by black arrows. H&E-stained sections **(A, E, F)** and X-ray images **(B)** are representative of $n = 2-5$ mice per genotype. Each symbol represents a datum from one individual mouse and error bars represent mean \pm SEM for $n = 8-25$. Hollowed-out symbols represent data from fighting male mice.

compared to wild-type controls at 3 months (Fig. 3A). Again, this difference was reflected in a 25% decrease in the average number of peripheral lymphocytes compared to wild-type littermate controls (Fig. 3B). Female *Ripk3*^{-/-} mice also exhibited a 47% decrease in their mean peripheral eosinophil population at 9 months when compared to wild-type littermate controls (Fig. 3E).

Mik1^{-/-} and *Ripk3*^{-/-} mice of both sexes displayed genotype-dependent differences in non-white blood cell hematological parameters. *Mik1*^{-/-} male mice showed significant increases in peripheral red blood cells (RBC) at 6 months when compared to wild-type littermate controls. Specifically, a 12% increase in the average absolute number and an 11% increase in the average ratio of RBC to the total volume of blood (percentage hematocrit) were observed at 6 months in comparison to littermate controls (Supplementary Fig. 3A, B). Fourteen-month-old *Mik1*^{-/-} male mice also showed a 7% increase in the average number of RBC when compared to wild-type littermate controls, however, this was not reflected in the percentage hematocrit (Supplementary Fig. 3A, B). Both *Mik1*^{-/-} and *Ripk3*^{-/-} mice displayed significant age-dependent variations in the hemoglobin potential of circulating RBC compared to wild-type littermate controls. Twelve-month-old male *Mik1*^{-/-} and 14-month-old female *Ripk3*^{-/-} mice displayed, respectively, a 9% and 44% decrease in mean corpuscular hemoglobin (MCH) measurements compared to their wild-type littermate controls (Supplementary Fig. 3C). Only *Mik1*^{-/-} mice displayed significant age-dependent differences in the size of the RBC. Whilst *Mik1*^{-/-} males showed a 2% increase in MCV at 3 months, 6- and 9-month-old *Mik1*^{-/-} females showed a 3% decrease and a 3% increase in MCV respectively, all compared to age-matched wild-type littermate controls (Supplementary Fig. 3D).

Finally, only *Mik1*^{-/-} mice displayed significant age-dependent differences in platelet parameters. By 12 months of age, *Mik1*^{-/-} females exhibited a 26% increase in the average number of peripheral platelets when compared to wild-type littermate controls (Supplementary Fig. 3E). When compared to wild-type littermate controls, 14-month-old *Mik1*^{-/-} females had a 12% decrease in mean platelet volume (MPV) and a corresponding 8% increase in mean platelet component (MPC) (Supplementary Fig. 3F, G). At 12 and 14 months of age, *Mik1*^{-/-} male mice had a 16% increase and 16% decrease, respectively in the MPV compared to wild-type littermate controls (Supplementary Fig. 3F). Consistent with these MPV findings, 12- and 14-month-old male *Mik1*^{-/-} mice also exhibited an 11% decrease and a 16% increase in MPC compared to wild-type littermate controls (Supplementary Fig. 3G). The observed variation in peripheral lymphocyte counts and other hematological parameters appear to be tolerated at steady state. However, whether these differences may be disease-causing during challenges that reflect an everyday human scenario, such as surgical blood loss, pregnancy, or chemotherapy ablation, remains to be investigated.

Bone marrow and splenic lymphocyte populations in female *Mik1*^{-/-} mice are comparable to wild-type littermate controls

There are many possible causes for the elevated number of circulating lymphocytes observed in aged *Mik1*^{-/-} mice, including

mobilisation from lymphoid organs, enhanced generation, enhanced lifespan, or reduced clearance. Splenic and bone marrow lymphocyte numbers, specifically—CD4⁺ T cells, CD8⁺ T cells and CD19⁺ B cells—in 12-month-old male and female *Mik1*^{-/-} mice showed no significant differences from their respective wild-type littermate controls (Fig. 4A, B, Supplementary Fig. 4A, B). Myeloid cell numbers in the spleen and bone marrow were also comparable across genotypes at 12 months (Fig. 4A, B, Supplementary Fig. 4A, B). Primary and secondary lymphoid organs were also assessed at 6 months to investigate whether there were any early signatures of lymphocytosis. Both male and female *Mik1*^{-/-} mice exhibited no significant differences in lymphocyte or myeloid cell counts in the bone marrow, spleen, and inguinal lymph nodes compared to wild-type littermate controls (Supplementary Fig. 4C–H). Quantification of lymphocyte populations did not provide insights as to the cause of increased peripheral lymphocyte numbers in female *Mik1*^{-/-} mice, therefore histological examination was performed for all lymphoid organs at an age before the onset of lymphocytosis. Both female *Mik1*^{-/-} and *Ripk3*^{-/-} mice displayed typical lymphoid organs that resembled their respective wild-type littermate controls at 9 months (Fig. 4C, Supplementary File 1).

Inflammatory aggregates in skeletal muscle and connective tissue of female *Mik1*^{-/-} mice are reduced at 17 months of age

Mik1^{-/-} mice exhibit a delayed age-driven reduction in circulating lymphocytes, so we questioned whether the absence of MLKL protects against other phenotypic hallmarks of aging. Veterinary histopathologists, blinded to genotype, examined the peripheral tissues of 9- and 17-month-old mice for evidence of inflammatory aggregates, a common finding in aging mice [51] (Fig. 5A, Supplementary File 1 and 2). At 9 months of age, male and female *Mik1*^{-/-} mice exhibited a similar degree of chronic sterile inflammation to wild-type littermate controls (Fig. 5B, Supplementary Fig. 5A). It was noted, however, that 9-month-old female *Mik1*^{-/-} mice exhibited an increasing trend in the total number of inflammatory foci in areas of skeletal muscle, bone, cartilage, adipose tissue, and connective tissue proper compared to wild-type littermate controls (Fig. 5C, Supplementary Fig. 5B). These foci were found in the head (excluding glandular and nervous tissue), hind leg, tail, sternum and the ventral skin of the abdomen (Supplementary Fig. 5C–G). By 17 months, however, female *Mik1*^{-/-} mice are protected against an age-dependent increase in sterile inflammation in skeletal muscle and connective tissue (Fig. 5A, C, Supplementary Fig. 5C–G). Compared to wild-type littermate controls, 17-month-old female *Mik1*^{-/-} mice exhibited a 62% reduction in the number of inflammatory foci observed in the combined skeletal muscle and connective tissue (Fig. 5C). This reduced number of inflammatory foci is not accompanied by any differences in the peripheral blood white blood cell populations, with comparable numbers of peripheral lymphocytes, neutrophils, monocytes, and eosinophils observed in 17-month-old *Mik1*^{-/-} females and wild-type littermate controls (Supplementary Fig. 5H).

With exception of the skeletal muscle and connective tissue, blinded examination of inflammatory foci numbers across 44 sites revealed no significant differences between genotypes or sex at 9

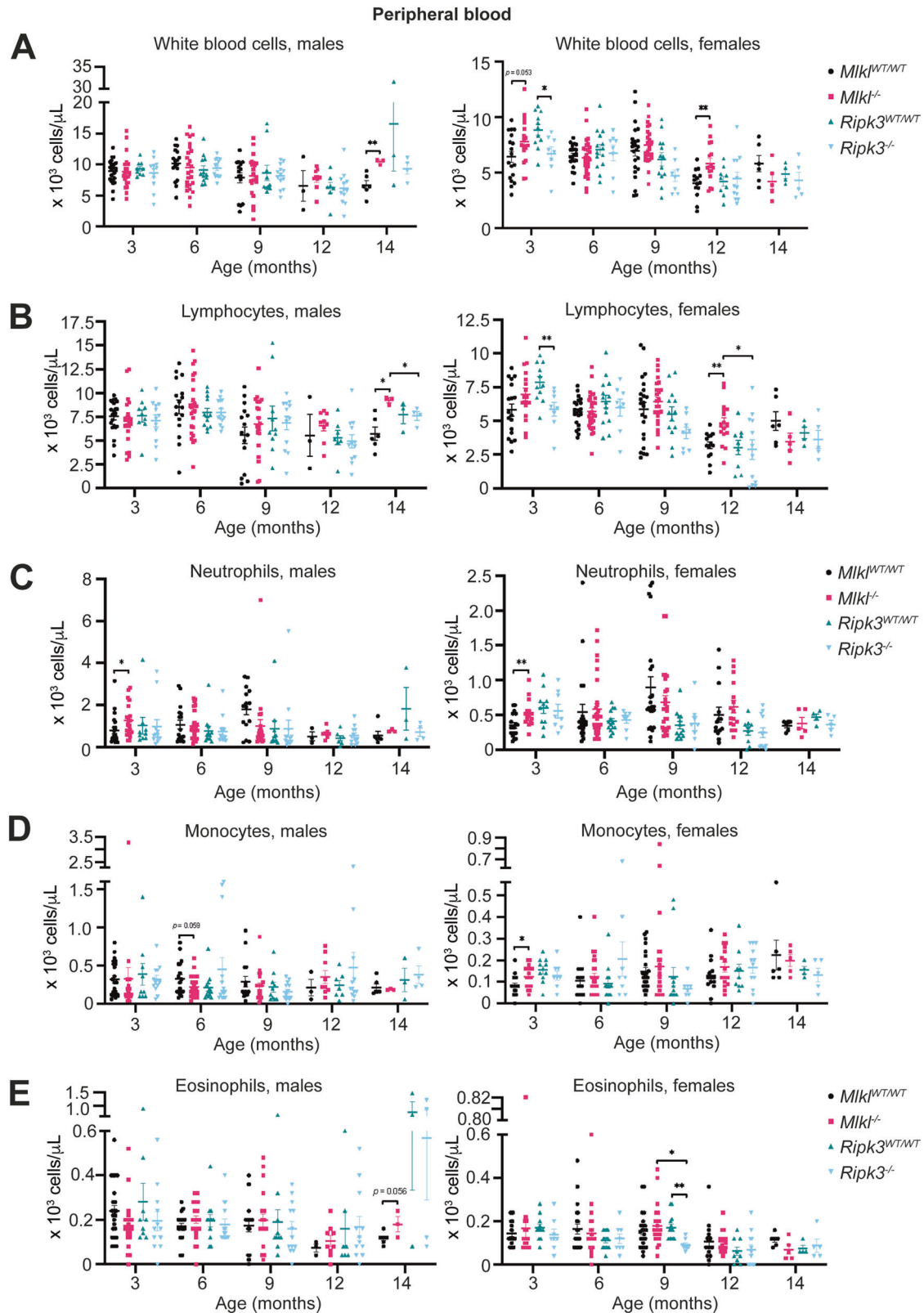


Fig. 3 Male and female *Mik1^{-/-}* mice exhibit increased circulating lymphocytes with age. ADVIA hematology quantification of circulating white blood cells (A), lymphocytes (B), neutrophils (C), monocytes (D) and eosinophils (E) in sex-separated *Mik1^{-/-}*, *Ripk3^{-/-}* and wild-type littermate control mice from 3 to 14 months of age. Each symbol represents a datum from one individual mouse and error bars represent mean \pm SEM for $n = 3 - 30$. * $p < 0.05$ and ** $p < 0.01$ were calculated using an unpaired, two-tailed Student's *t* test.

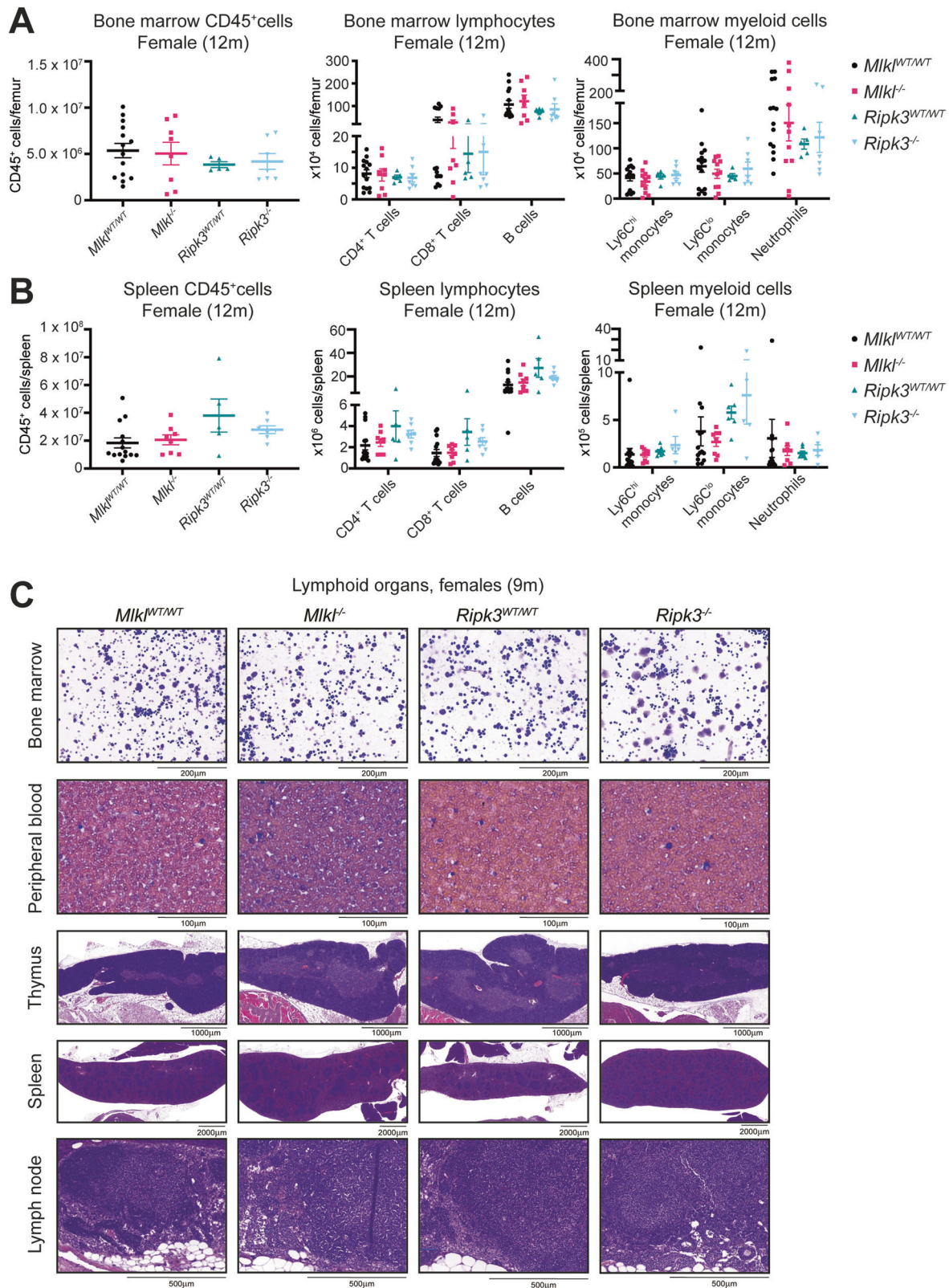
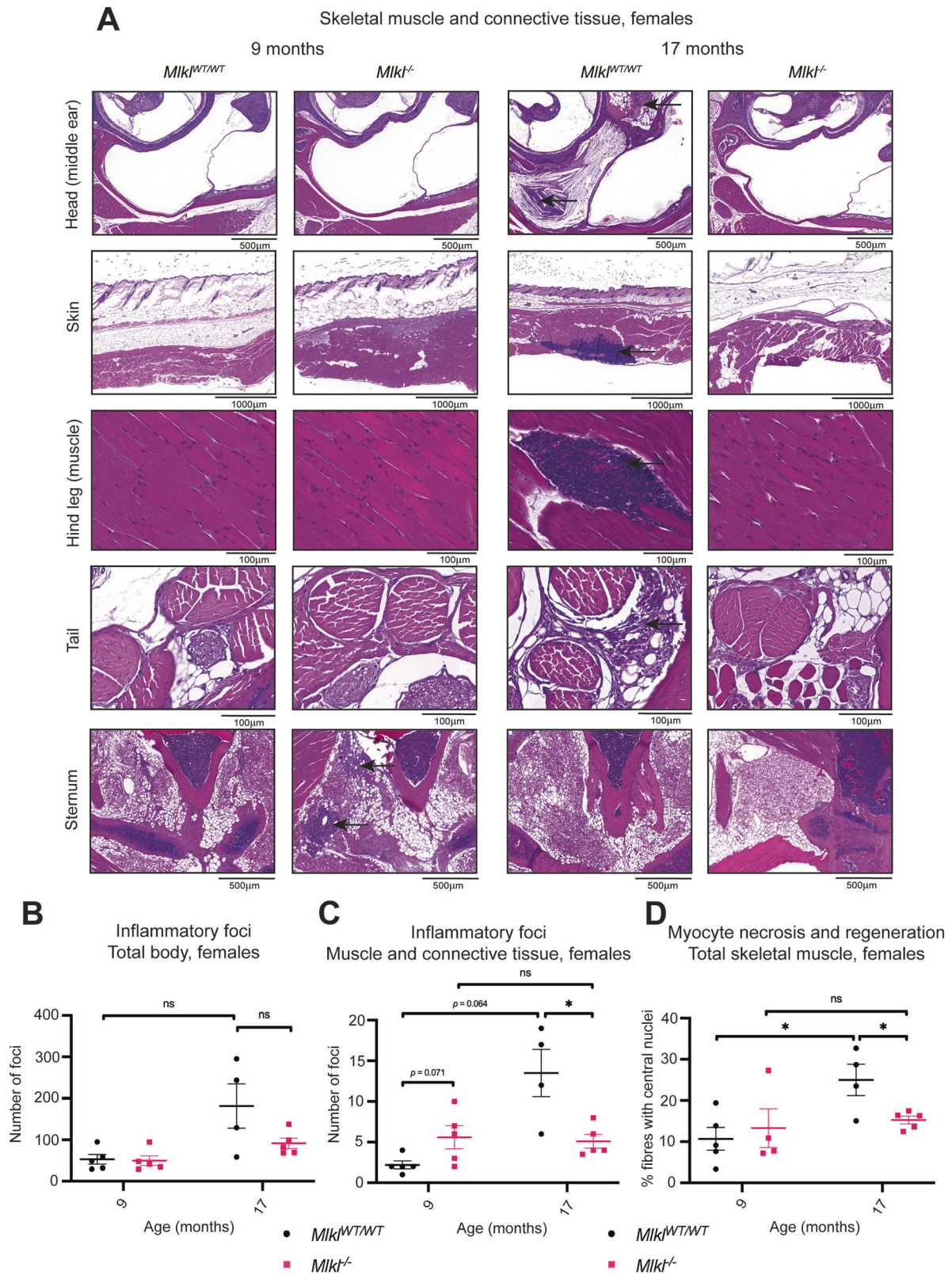


Fig. 4 Female *Mik1*^{-/-} mice have equivalent lymphocyte numbers in the spleen and bone marrow at 12 months of age. Quantification of CD45⁺ adaptive (CD4⁺ T cells, CD8⁺ T cells and B cells) and innate (Ly6C^{hi} monocytes, Ly6C^{lo} monocytes and neutrophils) immune cells in the bone marrow (A) and spleen (B) of 12-month-old female *Mik1*^{-/-}, *Ripk3*^{-/-} and wild-type littermate control mice. C H&E-stained sections of the lymphoid organs; bone marrow, peripheral blood, thymus, spleen, and lymph nodes in female *Mik1*^{-/-}, *Ripk3*^{-/-} and wild-type littermate control mice at 9 months of age. Sections are representative of $n = 2-6$ mice per genotype. Each symbol represents a datum from one individual mouse and error bars represent mean \pm SEM for $n = 5-14$.



and 17 months (Supplementary File 1 and 2). Specifically, inflammation was comparable irrespective of genotype and sex in tissues previously identified in MLKL-driven disease, such as the spinal cord, salivary glands, pancreas, liver, and kidney (Supplementary Fig. 5I – M, Supplementary Files 1 and 2).

It was previously reported that genetic knockout of *Mikl* in mice protects against muscle inflammation and necrosis in a model of myositis [52]. To determine whether an absence of MLKL is protective against age-dependent myocyte necrosis and subsequent regeneration, gastrocnemius, quadriceps, paraspinal and

Fig. 5 Female *Mkl1*^{-/-} mice are protected against chronic multifocal inflammation in connective and muscular tissue at 17 months of age. **A** Selected H&E sections of the head, skin, hind leg, tail, and sternum of 9- and 17-month-old female *Mkl1*^{WT/WT} and *Mkl1*^{-/-} mice. Inflammation is indicated by black arrows and H&E-stained sections are representative of $n = 4-5$ mice per genotype. **B** The total number of inflammatory foci identified in H&E-stained sections of all 44 sites across the body from female *Mkl1*^{WT/WT} and *Mkl1*^{-/-} mice. **C** The combined number of inflammatory foci identified in H&E-stained sections of the connective tissue and muscle that includes the head (excluding glandular and nervous tissue), hind leg, tail, skin, and sternum from female *Mkl1*^{WT/WT} and *Mkl1*^{-/-} mice. **D** The combined percentage of centralised nuclei (as an indicator of tissue regeneration) detected in gastrocnemius, quadriceps, paraspinal and gluteal muscles fibres of female *Mkl1*^{WT/WT} and *Mkl1*^{-/-} mice at 9 and 17 months. Each symbol represents a datum from one individual mouse and error bars display mean \pm SEM for $n = 4-5$ mice. * $p < 0.05$ calculated using the non-parametric Mann-Whitney U test (C; comparisons between 9- and 17-month groups) and unpaired, two-tailed Student's t test (C, D).

gluteal muscle sections from 9- and 17-month-old *Mkl1*^{-/-} and their wild-type littermate controls were examined. Specifically, muscle fibres were examined for centralised nuclei as an indicator of previous inflammation-related necrosis and subsequent regeneration. At 9 months, the percentage of centralised nuclei in the examined muscles was equivalent between *Mkl1*^{-/-} and wild-type controls of both sexes (Fig. 5D, Supplementary Fig. 6A-F). When quantified and plotted for each muscle group, there is a trend towards decreased muscle necrosis in 17-month-old female *Mkl1*^{-/-} mice compared to wild-type littermate controls (Supplementary Fig. 6A-D). When these muscle groups are combined, this difference becomes statistically significant; 17-month-old *Mkl1*^{-/-} female mice had 39% fewer muscle fibres with centralised nuclei compared to wild-type littermate controls (Fig. 5D).

DISCUSSION

Our extensive histopathological and immunophenotypic cohort analyses have identified several unique, sex-specific, differences between congenic C57BL/6J *Mkl1*^{-/-} and *Ripk3*^{-/-} mice and their wild-type littermates that emerge with age (Fig. 6). When measured as a percentage of body weight, male *Ripk3*^{-/-} mice had on average smaller, but histopathologically indistinguishable, spleens relative to wild-type littermate controls at 12 months. Several statistically significant findings were observed in hematological parameters across age in both *Mkl1*^{-/-} and *Ripk3*^{-/-} mice compared to wild-type littermate controls. Many of these parameters remained within normal range despite statistical significance, suggesting they are unlikely to assert biologically critical roles [53-55]. Of note, *Mkl1*^{-/-} mice exhibit increased circulating lymphocyte numbers relative to wild-type littermates at 12-14 months of age. A comprehensive and unbiased blind scoring of inflammatory foci in more than 44 different sites revealed a 62% decrease in background, sterile inflammation of the skeletal muscle, bone, cartilage, adipose tissue, and connective tissue proper in 17-month-old female *Mkl1*^{-/-} relative to age-matched wild-type littermates. It is important to consider, however, that these differences in age-related circulating lymphocyte numbers and tissue inflammation did not manifest in any overt differences in the general condition, mobility, or mortality of these mice up to 17 months of age.

"Inflammaging" is the chronic increase in basal sterile inflammation that is known to underpin a large range of age-related disease [56, 57]. Whilst the processes of inflammaging are not completely understood, mouse models that undergo accelerated aging, such as NF- κ B genetic knockouts, have provided clues to potential modulators and pathways [58, 59]. Furthermore, interventions in mice and humans intimately link anti-inflammatory effects and improved life span [60-62]. The significant reduction in the number of inflammatory foci in the skeletal muscle and connective tissue of 17-month-old *Mkl1*^{-/-} female mice suggests that removal of necroptosis, or another non-necroptotic role of MLKL, limits age-dependent sterile inflammation in C57BL/6J mice. At 17 months, *Mkl1*^{-/-} female mice also exhibited a reduced number of necrotic and regenerating myocytes. Together these data support recent reports that implicate MLKL and necroptosis

in muscle cell death and regeneration post inflammation or injury [52, 63]. Inflammaging is known to be closely linked with immunosenescence, the age-dependent decline in immune function [57, 64]. The observed increase in the numbers of circulating lymphocytes at 12 and 14 months in female and male *Mkl1*^{-/-} mice, respectively, could represent an interruption to the normal, age-dependent reduction in circulating lymphocytes in C57BL/6J mice [55]. Normalization of the lymphocyte parameters at 14 months in female *Mkl1*^{-/-} mice is suggestive that the absence of MLKL may delay these age-related changes, rather than halt them completely. Our observations of both delayed age-related lymphocytosis and reduced focal inflammation are suggestive that MLKL's absence may impede select features of the aging process.

In the past four years, three previous reports have implicated human MLKL loss-of-function mutations in neurodegenerative or diabetic disease [45-47]. We did not detect evidence of either condition in appropriately aged *Mkl1*^{-/-} and *Ripk3*^{-/-} mice in this study. One such reason for this could be the approaches used here for screening of disease pathologies, given there are more specific and accurate tests that could have been employed to identify nuanced phenotypes [49, 65, 66]. Nevertheless, we note that syndromes akin to the reports of severe human disease in patients with MLKL substitutions would have been detected in the current investigation. More likely, these human reports capture MLKL deficiency "in the real world", where mutations occur alongside other genetic and/or environmental insults that are not consistent between individuals in the way that they are in laboratory mice. For example, in the two patients suffering from neurodegeneration, the MLKL loss-of-function mutation (*p.Asp369GlufsTer22*) also segregated with homozygous mutations in the *FA2H* and *ASP152* genes, which have each been linked to severe neurological syndromes [67-69]. Similarly, in the case of MODY diabetes, the heterozygous MLKL loss-of-function mutation also segregated with heterozygous deleterious mutations in the known MODY gene *PDX1*, as well as *ERN2*, *NIPAL4* and *SPTBN4* in affected individuals [47]. Whilst our investigations of *Mkl1*^{-/-} mice did not unveil any neurodegenerative or diabetic disease, it would be of interest to identify whether MLKL loss-of-function carriers presented with the phenotypes identified in our mice. Specifically, none of the three clinical reports provided information on the peripheral blood parameters of patients and it would be informative to know if, consistent with *Mkl1* knockout mice, they exhibit increased peripheral lymphocyte numbers. While it is likely that genetic context is critical to reveal patient phenotypes, whether our observed age-related changes in metabolic, hematological, and inflammatory parameters may act as modifiers of disease in the presence of physiological challenge is yet to be established.

Therapeutic targeting of the necroptotic signaling pathway is of immense clinical interest, exemplified by the active clinical trials of RIPK1-targeted small molecule compounds [42-44]. Despite no current first-in-human trials for RIPK3 or MLKL targeted drugs, their integral role in necroptosis makes them highly desirable potential targets (clinicaltrials.gov; accessed on 13 September 2022). The age-dependent phenotypes that we observed in *Mkl1*^{-/-} mice highlight that long-term inhibition may have several

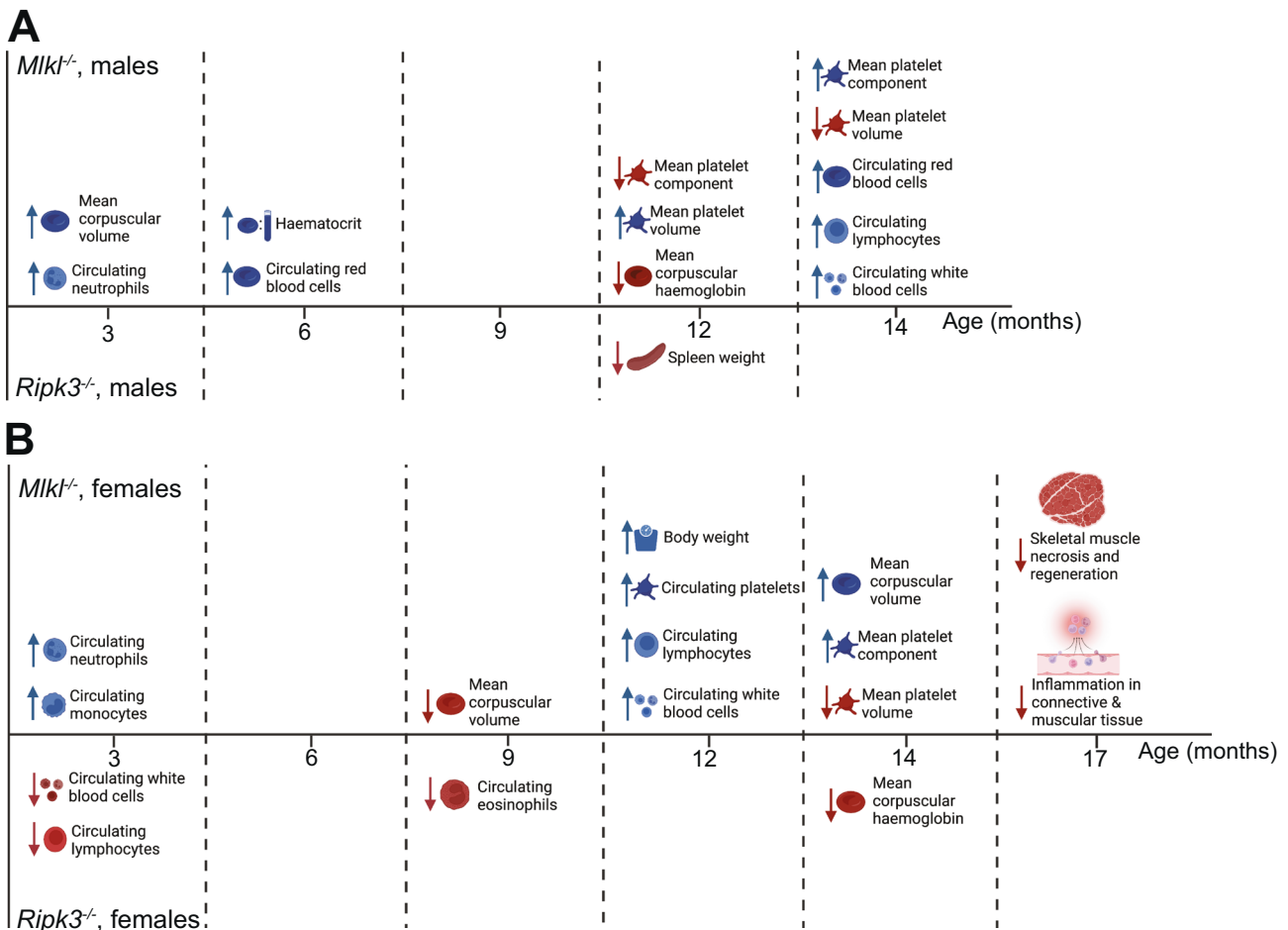


Fig. 6 Summary of the identified phenotypic differences in *MIK1^{-/-}* and *Ripk3^{-/-}* mice compared with age- and sex-matched wild-type littermate controls. **A Male *MIK1^{-/-}* mice exhibit differences in circulating blood cell parameters at 3, 6, 12 and 14 months of age. *Ripk3^{-/-}* male mice exhibit a decrease in spleen weight at 12 months of age. **B** Both *MIK1^{-/-}* and *Ripk3^{-/-}* females displayed phenotypes in the circulating blood at 3, 9 and 14 months. Only *MIK1^{-/-}* females exhibited significant phenotypes in the circulating blood and an increase in body weight at 12 months. Seventeen-month-old *MIK1^{-/-}* females also exhibit a significant decrease in the number of inflammatory foci identified in skeletal muscle and connective tissue alongside a significant decrease in the number of regenerating myocytes.**

important age-related health benefits. However, differing age-related phenotypes in *Ripk3^{-/-}* and *MIK1^{-/-}* mice suggest there are advantages to therapeutically targeting RIPK3 or MLKL depending on the disease context. Our study provides provocative evidence of age-related MLKL and RIPK3 roles that will be of immense interest as anti-necroptotic inhibitors advance toward the clinic.

METHODS

Mice

All mice used in this study were housed at a temperature and humidity-controlled facility at The Walter and Eliza Hall Institute of Medical Research (WEHI). Operating on a 12 h:12 h day-night cycle, this is a specific pathogen-free facility. The generation of the *MIK1^{-/-}* mice used in this study was reported previously [4]. The *Ripk3^{-/-}* mice were generated by the MAGEC laboratory (WEHI) on a C57BL/6J background. To generate the *Ripk3^{-/-}* mice, 20 ng/μl of Cas9 mRNA, and 10 ng/μl of sgRNAs (AACTTGACAGAAGACATCGT and GATTCTCTGAAGTCTACTTG; targeting the 5' UTR-Exon1 and Exon 10-3' UTR junctions, respectively, for deletion of the intervening locus) were injected into the cytoplasm of fertilized one-cell stage embryos generated from wild-type C57BL/6J breeders. Twenty-four hours later, two-cell stage embryos were transferred into the uteri of pseudo-pregnant female mice. Viable offspring were genotyped by next-generation sequencing. Targeted animals were backcrossed twice to wild-type C57BL/6J to eliminate off-target mutations. Mice aged to 3 months were between 13 and 16 weeks, 6 months between 26 and 30 weeks,

9 months between 35 and 43 weeks, 12 months between 48 and 60 weeks except for ADVIA data where mice were aged between 49 and 58 weeks, 14 months between 60 and 64 weeks of age and 17 months between 73 and 75 weeks. Mice were checked twice weekly until 52 weeks old, after which they were checked three times weekly. All mice in this study were housed within the same facility, with genetic knockout mice housed in the same room as their wild-type littermate controls. *MIK1^{-/-}* and *Ripk3^{-/-}* colonies were maintained in different rooms within the same facility. Because knockout and wild-type littermates were matched to specific rooms and no challenges were performed on the mice, cohorts were not randomized. Cohort sizes were typical of other studies examining the role of necroptosis deficiency in aging [33].

Hematological analysis

Cardiac or sub-mandibular blood from mice aged between 3 and 17 months was collected into EDTA-coated tubes. Blood was diluted between 2- and 10-fold in DPBS for automated blood cell quantification using an ADVIA 2120i hematological analyzer on the same day as harvest. Accu-Chek Performa Blood Glucose Meter measured blood glucose on undiluted blood within 2 hours of harvest. Any mice that had been observed fighting and exhibited overt skin wounds resulting from fighting were excluded from hematological analyses.

Whole body histopathology, 9 and 17 months of age

Comprehensive histological examinations of 9-month-old male and female *MIK1^{WT/WT}*, *MIK1^{-/-}*, *Ripk3^{WT/WT}*, and *Ripk3^{-/-}* mice and 17-month-old female

Mkl1^{WT/WT} and *Mkl1^{-/-}* mice were completed by histopathologists at Phenomics Australia, Melbourne. 9-month-old mice were dispatched to Phenomics Australia in separate cohorts, whilst 17-month-old female mice were all dispatched in one singular cohort on the same day. Mice were euthanized by CO₂ inhalation. All soft tissues, except for testes, epididymides, eyes and Harderian glands, were placed into 10% v/v neutral buffered formalin (NBF) for 24 hours before being transferred into 10% v/v NBF. Testes and epididymides were placed into Bouin's fixative and the eyes and Harderian glands into Davidson's fixative. Skeletal tissues were fixed for 48 h in 10% v/v NBF, followed by 48 h of 10% v/v formic acid for decalcification and then back into 10% v/v NBF for a further 24 h. Following fixation, tissues were moved for automated processing to paraffin using the Sakura VIP6 auto processor. Paraffin blocks of embedded tissues were sectioned at 5 µm thickness, with one representative section taken through the entire tissue. Sections were stained with hematoxylin and eosin on the Leica Autostainer XL/Leica CV5030 coverslipper. X-rays were obtained using the portable X-ray system iRayD3 (DX-3000L).

Trained histopathologists examined all tissues from mice at 9 or 17 months of age for inflammation, quantifying the number of inflammatory foci in each section, blinded to genotype. The size of the brain was quantified by measuring the length, width, and height. Senior Veterinary Pathologist, Prof. John W. Finnie from the School of Medicine, University of Adelaide performed a detailed neuropathological examination on all mice and confirmed the full body findings for all 9-month-old mice. Senior Veterinary Pathologist, Dr Lorna Rasmussen confirmed the full body findings for all 17-month-old mice.

Myocyte regeneration scoring

Morphological features of the quadriceps, tibialis anterior, gluteal and paraspinal muscles were assessed in a blinded fashion using digital images of H&E-stained sections. Sections were performed at standardized levels for all mice. Non-overlapping fields were analyzed to ensure the entire muscle area was assessed. Manual counting of muscle fibres was performed and the percentage of fibres with centralized nuclei (as an indicator of previously necrotic and regenerated tissue) was determined according to SOP DMD_M.1.2.007.

Organ tissue harvest and processing, 12 months of age

Twelve-month-old mice were euthanized by CO₂ inhalation immediately before organ dissection. Each organ was weighed before fixation in 10% v/v neutral buffered formalin and long-term storage in 80% v/v ethanol. Mice that had been observed fighting and exhibited overt skin wounds resulting from fighting were plotted as hollowed-out symbols. H&E staining of harvested spleen was completed by the WEHI Histology Facility. Heart, colon, ileum, spleen, testes, and liver organ samples taken from 12-month-old mice were lysed in ice-cold RIPA buffer supplemented with Protease & Phosphatase Inhibitor Cocktail (Cell Signaling Technology 5872 S, 50 mg/ml) and Benzonase (Sigma-Aldrich E1014, 100 U/mL). Tissue lysates were homogenized using the Qiagen TissueLyser II (30 Hz, 1 min). Proteins were harvested in 2 x SDS-loading buffer and visualised as per the western blot protocol below.

Flow cytometry

To analyze immune cells (innate and adaptive) in the spleen, bone marrow or inguinal lymph nodes of 6- and 12-month-old *Mkl1^{WT/WT}*, *Mkl1^{-/-}*, *Ripk3^{WT/WT}*, and *Ripk3^{-/-}* mice, single-cell suspensions were subjected to osmotic red blood cell lysis and incubated with a combination of antibodies: CD4-BV421 (BD Biosciences #562891), CD8-PeCy7 (BD Biosciences #561097), CD19-PerCPCy5.5 (BD Biosciences #551001), CD11b-BV510 (BD Biosciences #562950) or CD11b-BV786 (BD Biosciences #740861), CD45-Alexa700 (BD Biosciences #560566), Ly6G-V450 (BD Biosciences #560603) and Ly6C-APCCy7 (BD Biosciences #560596). Samples were analyzed on an Aurora Cytex flow cytometer, with the automated volume calculator used to quantify absolute cell numbers. FlowJo v10.8 was used for all analyses.

Cell line generation and maintenance

Primary mouse dermal fibroblasts (MDFs) were prepared from the skin taken from the tails of 6-week-old *Ripk3^{WT/WT}* or *Ripk3^{-/-}* mice. Primary MDFs were immortalized by stable lentiviral transduction with a DNA construct encoding the SV40 large T antigen, using established procedures [4]. MDFs were cultured in Dulbecco's Modified Eagle Medium (DMEM) + 8% (v/v) fetal calf serum (FCS) at 37 °C with 10% CO₂. Cell lines were routinely monitored for mycoplasma.

IncuCyte cell death assays

MDFs were seeded into 96-well plates at 8×10^3 cells/well and left to settle for 6 h. The next day, MDFs were stimulated in Phenol Red-free DMEM (ThermoFisher Scientific) supplemented with 2% FCS, 1 mM L-GlutaMAX, G/P/S, 1 mM Na pyruvate, SYTOX Green (5 µM; Invitrogen S7020) and DRAQ5 (10 µM; ThermoFisher #62251). MDFs were stimulated with combination treatments of TNF (100 ng/mL), Smac-mimetic compound A (500 nM; TS) or TS plus pan-caspase inhibitor IDN-6556 (5 µM; TSI), in the absence or presence of RIPK3 inhibitor GSK'872 (1 µM). Cells were moved into an SX5 system (37 °C, 10% CO₂; Essen Bioscience) and imaged with a ×10 objective every hour. Percentage cell death values were quantified by the number of dead cells (SYTOX Green-positive) out of the total live cell number (DRAQ5 positive) using the IncuCyte v.2022 A software.

Western blot

Immortalized MDFs were plated at 3×10^4 cells/well and left to adhere overnight. The next day, cells were stimulated as indicated with a combination of treatments TNF (100 ng/mL), Smac-mimetic Compound A (500 nM), pan-caspase inhibitor IDN-6556 (5 µM), and GSK'872 (1 µM) for 4 h. All cells were harvested in 2 x SDS Laemmli lysis buffer and boiled at 100 °C for 10–15 min. Proteins were resolved by 4–15% Tris-Glycine gel (Bio-Rad) and transferred to nitrocellulose membrane, before probing with indicated antibodies. Uncropped blots are included as supplemental data.

Reagents

Antibodies: Rat anti-mMLKL 5A6 and rat anti-mRIPK3 1H12 were produced in-house [70] (5A6 available from Merck as MABC1634). Mouse anti-actin (A-1978) was purchased from Sigma-Aldrich, rabbit anti-mouse pMLKL (D6E3G) was purchased from CST and rabbit anti-mouse pRIPK3 (GEN135-35-9) was kindly provided by Genentech [71]. Recombinant human TNF-Fc (produced in-house) and the Smac mimetic, Compound A, have been previously described [72, 73]. Pan-caspase inhibitor IDN-6556 was provided by Tetralogic Pharmaceuticals and GSK'872 was sourced from SynKinase.

Statistical analysis

All data points signify independent experimental repeats, and/or biologically independent repeats. All *p* values were calculated in Prism using an unpaired, two-tailed Student's *t* test or non-parametric Mann-Whitney U test as indicated. Asterisks signify that $p \leq 0.05$ (*), $p \leq 0.01$ (**), $p \leq 0.001$ (***)

DATA AVAILABILITY

All primary data are available from the corresponding authors on request.

REFERENCES

- Weir A, Hughes S, Rashidi M, Hildebrand JM, Vince JE. Necroptotic movers and shakers: cell types, inflammatory drivers and diseases. *Curr Opin Immunol.* 2021;68:83–97.
- Sun L, Wang H, Wang Z, He S, Chen S, Liao D, et al. Mixed lineage kinase domain-like protein mediates necrosis signaling downstream of RIP3 kinase. *Cell.* 2012;148:213–27.
- Zhao J, Jitkaew S, Cai Z, Choksi S, Li Q, Luo J, et al. Mixed lineage kinase domain-like is a key receptor interacting protein 3 downstream component of TNF-induced necrosis. *Proc Natl Acad Sci USA.* 2012;109:5322–7.
- Murphy JM, Czabotar PE, Hildebrand JM, Lucet IS, Zhang JG, Alvarez-Diaz S, et al. The pseudokinase MLKL mediates necroptosis via a molecular switch mechanism. *Immunity.* 2013;39:443–53.
- Cai Z, Jitkaew S, Zhao J, Chiang HC, Choksi S, Liu J, et al. Plasma membrane translocation of trimerized MLKL protein is required for TNF-induced necroptosis. *Nat Cell Biol.* 2014;16:55–65.
- Chen X, Li W, Ren J, Huang D, He WT, Song Y, et al. Translocation of mixed lineage kinase domain-like protein to plasma membrane leads to necrotic cell death. *Cell Res.* 2014;24:105–21.
- Dondelinger Y, Declercq W, Montessuit S, Roelandt R, Goncalves A, Bruggeman I, et al. MLKL compromises plasma membrane integrity by binding to phosphatidylinositol phosphates. *Cell Rep.* 2014;7:971–81.
- Hildebrand JM, Tanzer MC, Lucet IS, Young SN, Spall SK, Sharma P, et al. Activation of the pseudokinase MLKL unleashes the four-helix bundle domain to induce membrane localization and necroptotic cell death. *Proc Natl Acad Sci USA.* 2014;111:15072–7.

9. Wang H, Sun L, Su L, Rizo J, Liu L, Wang LF, et al. Mixed lineage kinase domain-like protein MLKL causes necrotic membrane disruption upon phosphorylation by RIP3. *Mol Cell*. 2014;54:133–46.
10. Samson AL, Zhang Y, Geoghegan ND, Gavin XJ, Davies KA, Mlodzianoski MJ, et al. MLKL trafficking and accumulation at the plasma membrane control the kinetics and threshold for necroptosis. *Nat Commun*. 2020;11:3151.
11. Li D, Meng L, Xu T, Su Y, Liu X, Zhang Z, et al. RIPK1-RIPK3-MLKL-dependent necrosis promotes the aging of mouse male reproductive system. *Elife*. 2017;6:e27692.
12. Wu J, Huang Z, Ren J, Zhang Z, He P, Li Y, et al. Mkl1 knockout mice demonstrate the indispensable role of Mkl1 in necroptosis. *Cell Res*. 2013;23:994–1006.
13. Alvarez-Diaz S, Dillon CP, Lalaoui N, Tanzer MC, Rodriguez DA, Lin A, et al. The pseudokinase MLKL and the kinase RIPK3 have distinct roles in autoimmune disease caused by loss of death-receptor-induced apoptosis. *Immunity*. 2016;45:513–26.
14. Newton K, Sun X, Dixit VM. Kinase RIP3 is dispensable for normal NF- κ Bs, signaling by the B-cell and T-cell receptors, tumor necrosis factor receptor 1, and Toll-like receptors 2 and 4. *Mol Cell Biol*. 2004;24:1464–9.
15. Linkermann A, Skouta R, Himmerkus N, Mulay SR, Dewitz C, De Zen F, et al. Synchronized renal tubular cell death involves ferroptosis. *Proc Natl Acad Sci USA*. 2014;111:16836–41.
16. Newton K, Dugger DL, Maltzman A, Greve JM, Hedehus M, Martin-McNulty B, et al. RIPK3 deficiency or catalytically inactive RIPK1 provides greater benefit than MLKL deficiency in mouse models of inflammation and tissue injury. *Cell Death Differ*. 2016;23:1565–76.
17. Mullin BH, Tickner J, Zhu K, Kenny J, Mullin S, Brown SJ, et al. Characterisation of genetic regulatory effects for osteoporosis risk variants in human osteoclasts. *Genome Biol*. 2020;21:80.
18. Tanzer MC, Tripaydonis A, Webb AI, Young SN, Varghese LN, Hall C, et al. Necroptosis signalling is tuned by phosphorylation of MLKL residues outside the pseudokinase domain activation loop. *Biochemical J*. 2015;471:255–65.
19. Kitur K, Wachtel S, Brown A, Wickersham M, Paulino F, Penalzo HF, et al. Necroptosis Promotes Staphylococcus aureus Clearance by Inhibiting Excessive Inflammatory Signaling. *Cell Rep*. 2016;16:2219–30.
20. D'Cruz AA, Speir M, Bliss-Moreau M, Dietrich S, Wang S, Chen AA, et al. The pseudokinase MLKL activates PAD4-dependent NET formation in necroptotic neutrophils. *Sci Signal*. 2018;11:eaao1716.
21. Muller T, Dewitz C, Schmitz J, Schroder AS, Brasen JH, Stockwell BR, et al. Necroptosis and ferroptosis are alternative cell death pathways that operate in acute kidney failure. *Cell Mol Life Sci*. 2017;74:3631–45.
22. Rickard JA, Anderton H, Etemadi N, Nachbur U, Darding M, Peltzer N, et al. TNFR1-dependent cell death drives inflammation in Sharpin-deficient mice. *Elife*. 2014;3:e03464.
23. Devos M, Tanghe G, Gilbert B, Dierick E, Verheirstraeten M, Nemegeer J, et al. Sensing of endogenous nucleic acids by ZBP1 induces keratinocyte necroptosis and skin inflammation. *J Exp Med*. 2020;217:e20191913.
24. Tovey Crutchfield EC, Garnish SE, Hildebrand JM. The role of the key effector of necroptotic cell death, MLKL, in mouse models of disease. *Biomolecules*. 2021;11:803.
25. Lawlor KE, Khan N, Mildenhall A, Gerlic M, Croker BA, D'Cruz AA, et al. RIPK3 promotes cell death and NLRP3 inflammasome activation in the absence of MLKL. *Nat Commun*. 2015;6:6282.
26. Conos SA, Chen KW, De Nardo D, Hara H, Whitehead L, Nunez G, et al. Active MLKL triggers the NLRP3 inflammasome in a cell-intrinsic manner. *Proc Natl Acad Sci USA*. 2017;114:E961–E969.
27. Mandal P, Berger SB, Pillay S, Moriwaki K, Huang C, Guo H, et al. RIP3 induces apoptosis independent of pro-necrotic kinase activity. *Mol Cell*. 2014;56:481–95.
28. Newton K, Dugger DL, Wickliffe KE, Kapoor N, de Almagro MC, Vucic D, et al. Activity of protein kinase RIPK3 determines whether cells die by necroptosis or apoptosis. *Science*. 2014;343:1357–60.
29. Rebsamen M, Heinz LX, Meylan E, Michallet MC, Schroder K, Hofmann K, et al. DAI/ZBP1 recruits RIP1 and RIP3 through RIP homotypic interaction motifs to activate NF- κ B. *EMBO Rep*. 2009;10:916–22.
30. Wong WW, Vince JE, Lalaoui N, Lawlor KE, Chau D, Bankovacki A, et al. cIAPs and XIAP regulate myelopoiesis through cytokine production in an RIPK1- and RIPK3-dependent manner. *Blood*. 2014;123:2562–72.
31. Vanden Berghe T, Hulpiau P, Martens L, Vandenbroucke Roosmarijn E, Van Woutherghem E, Perry Seth W, et al. Passenger mutations confound interpretation of all genetically modified congenic mice. *Immunity*. 2015;43:200–9.
32. Eisfeld AJ, Gasper DJ, Suresh M, Kawaoka Y. C57BL/6J and C57BL/6NJ mice are differentially susceptible to inflammation-associated disease caused by influenza A virus. *Front Microbiol*. 2019;9:3307.
33. Webster JD, Kwon YC, Park S, Zhang H, Corr N, Ljumanovic N, et al. RIP1 kinase activity is critical for skin inflammation but not for viral propagation. *J Leukoc Biol*. 2020;107:941–52.
34. Hildebrand JM, Kauppi M, Majewski IJ, Liu Z, Cox AJ, Miyake S, et al. A missense mutation in the MLKL brace region promotes lethal neonatal inflammation and hematopoietic dysfunction. *Nat Commun*. 2020;11:3150.
35. Lalaoui N, Boyden SE, Oda H, Wood GM, Stone DL, Chau D, et al. Mutations that prevent caspase cleavage of RIPK1 cause autoinflammatory disease. *Nature*. 2020;577:103–8.
36. Karunakaran D, Geoffrion M, Wei L, Gan W, Richards L, Shangari P, et al. Targeting macrophage necroptosis for therapeutic and diagnostic interventions in atherosclerosis. *Sci Adv*. 2016;2:e1600224. p
37. Hu YB, Zhang YF, Wang H, Ren RJ, Cui HL, Huang WY, et al. miR-425 deficiency promotes necroptosis and dopaminergic neurodegeneration in Parkinson's disease. *Cell Death Dis*. 2019;10:589.
38. Oñate M, Catenaccio A, Salvadores N, Saquel C, Martinez A, Moreno-Gonzalez I, et al. Correction: The necroptosis machinery mediates axonal degeneration in a model of Parkinson disease. *Cell Death Differ*. 2020;27:2294.
39. Caccamo A, Branca C, Piras IS, Ferreira E, Huentelman MJ, Liang WS, et al. Necroptosis activation in Alzheimer's disease. *Nat Neurosci*. 2017;20:1236–46.
40. Koper MJ, Van Schoor E, Ospitalieri S, Vandenbergh R, Vandenbulcke M, von Arnim CAF, et al. Necrosome complex detected in granulovacuolar degeneration is associated with neuronal loss in Alzheimer's disease. *Acta Neuropathologica*. 2020;139:463–84.
41. Ofengeim D, Ito Y, Najafov A, Zhang Y, Shan B, DeWitt JP, et al. Activation of necroptosis in multiple sclerosis. *Cell Rep*. 2015;10:1836–49.
42. Weisel K, Berger S, Thorn K, Taylor PC, Peterfy C, Siddall H, et al. A randomized, placebo-controlled experimental medicine study of RIPK1 inhibitor GSK2982772 in patients with moderate to severe rheumatoid arthritis. *Arthritis Res Ther*. 2021;23:85.
43. Sanofi. Phase 2 Study for SAR443820 in Participants With Amyotrophic Lateral Sclerosis (ALS) (HIMALAYA). 2022 [cited] Available from: <https://clinicaltrials.gov/ct2/show/NCT05237284?term=Himalaya&draw=2&rank=4>.
44. GlaxoSmithKline. First-time-in-human (FTIH) Study of GSK3145095 Alone and in Combination With Other Anticancer Agents in Adults With Advanced Solid Tumors. 2018 [cited] Available from: <https://clinicaltrials.gov/ct2/show/results/NCT03681951>.
45. Wang B, Bao S, Zhang Z, Zhou X, Wang J, Fan Y, et al. A rare variant in MLKL confers susceptibility to ApoE ϵ 4-negative Alzheimer's disease in Hong Kong Chinese population. *Neurobiol Aging*. 2018;68:160.e161–160.e167.
46. Faergeman SL, Evans H, Attfield KE, Desel C, Kuttikkatte SB, Sommerlund M, et al. A novel neurodegenerative spectrum disorder in patients with MLKL deficiency. *Cell Death Dis*. 2020;11:303.
47. Hildebrand JM, Lo B, Tomei S, Mattei V, Young SN, Fitzgibbon C, et al. A family harboring an MLKL loss of function variant implicates impaired necroptosis in diabetes. *Cell Death Dis*. 2021;12:345.
48. [Jax] TJL. Life span as a biomarker Gerontology: mechanisms of aging 2021 [cited 2021 01/06] Available from: <https://www.jax.org/research-and-faculty/research-labs/the-harrison-lab/gerontology/life-span-as-a-biomarker>.
49. Steru L, Chermat R, Thierry B, Simon P. The tail suspension test: A new method for screening antidepressants in mice. *Psychopharmacology*. 1985;85:367–70.
50. Kelly RR, Sidles SJ, LaRue AC. Effects of neurological disorders on bone health. *Front Psychol*. 2020;11:612366.
51. Maronpot RR, Boorman GA, Gaul BW. *Pathology of the mouse: reference and atlas*. Cache River Press: Vienna, IL, 1999.
52. Kamiya M, Mizoguchi F, Kawahata K, Wang D, Nishibori M, Day J, et al. Targeting necroptosis in muscle fibers ameliorates inflammatory myopathies. *Nat Commun*. 2022;13:166.
53. Mazzaccara C, Labruna G, Cito G, Scarfò M, De Felice M, Pastore L, et al. Age-related reference intervals of the main biochemical and hematological parameters in C57BL/6J, 129SV/EV and C3H/HeJ mouse strains. *PLoS One*. 2008;3:e3772.
54. Silva-Santana G, Bax JC, Fernandes DCS, Bacellar DTL, Hooper C, Dias A, et al. Clinical hematological and biochemical parameters in Swiss, BALB/c, C57BL/6 and B6D2F1 Mus musculus. *Anim Model Exp Med*. 2020;3:304–15.
55. Grubb SC, Bult CJ, Bogue MA. Mouse phenome database. *Nucleic Acids Res*. 2014;42:D825–834.
56. Kennedy BK, Berger SL, Brunet A, Campisi J, Cuervo AM, Epel ES, et al. Geroscience: linking aging to chronic disease. *Cell*. 2014;159:709–13.
57. Franceschi C, Bonafè M, Valensin S, Olivieri F, De Luca M, Ottaviani E, et al. Inflamm-aging. An evolutionary perspective on immunosenescence. *Ann N Y Acad Sci*. 2000;908:244–54.
58. Jurk D, Wilson C, Passos JF, Oakley F, Correia-Melo C, Greaves L, et al. Chronic inflammation induces telomere dysfunction and accelerates ageing in mice. *Nat Commun*. 2014;2:4172.
59. Marin-Aguilar F, Lechuga-Vieco AV, Alcocer-Gomez E, Castejon-Vega B, Lucas J, Garrido C, et al. NLRP3 inflammasome suppression improves longevity and prevents cardiac aging in male mice. *Aging Cell*. 2020;19:e13050.

60. Burska AN, Sakthiswary R, Sattar N. Effects of tumour necrosis factor antagonists on insulin sensitivity/resistance in rheumatoid arthritis: a systematic review and meta-analysis. *PLoS One*. 2015;10:e0128889.
61. Chou RC, Kane M, Ghimire S, Gautam S, Gui J. Treatment for rheumatoid arthritis and risk of alzheimer's disease: a nested case-control analysis. *CNS Drugs*. 2016;30:1111–20.
62. Royce GH, Brown-Borg HM, Deepa SS. The potential role of necroptosis in inflammaging and aging. *Geroscience*. 2019;41:795–811.
63. Zhou SA, Zhang W, Cai G, Ding Y, Wei C, Li S, et al. Myofiber necroptosis promotes muscle stem cell proliferation via releasing Tenascin-C during regeneration. *Cell Res*. 2020;30:1063–77.
64. Bauer ME, Fuente Mde L. The role of oxidative and inflammatory stress and persistent viral infections in immunosenescence. *Mech Ageing Dev*. 2016;158:27–37.
65. Vogel AP, Tsanas A, Scattoni ML. Quantifying ultrasonic mouse vocalizations using acoustic analysis in a supervised statistical machine learning framework. *Sci Rep*. 2019;9:8100.
66. Ayala JE, Samuel VT, Morton GJ, Obici S, Croniger CM, Shulman GI, et al. Standard operating procedures for describing and performing metabolic tests of glucose homeostasis in mice. *Dis Model Mech*. 2010;3:525–34.
67. Edvardson S, Hama H, Shaag A, Gomori JM, Berger I, Soffer D, et al. Mutations in the fatty acid 2-hydroxylase gene are associated with leukodystrophy with spastic paraparesis and dystonia. *Am J Hum Genet*. 2008;83:643–8.
68. Cacciagli P, Desvignes J-P, Girard N, Delepine M, Zelenika D, Lathrop M, et al. AP1S2 is mutated in X-linked Dandy-Walker malformation with intellectual disability, basal ganglia disease and seizures (Pettigrew syndrome). *Eur J Hum Genet*. 2014;22:363–8.
69. Ballarati L, Cereda A, Caselli R, Maitz S, Russo S, Selicorni A, et al. Deletion of the AP1S2 gene in a child with psychomotor delay and hypotonia. *Eur J Med Genet*. 2012;55:124–7.
70. Samson AL, Fitzgibbon C, Patel KM, Hildebrand JM, Whitehead LW, Rimes JS, et al. A toolbox for imaging RIPK1, RIPK3, and MLKL in mouse and human cells. *Cell Death Differ*. 2021;28:2126–44.
71. Newton K, Wickliffe KE, Maltzman A, Dugger DL, Strasser A, Pham VC, et al. RIPK1 inhibits ZBP1-driven necroptosis during development. *Nature*. 2016;540:129–33.
72. Bossen C, Ingold K, Tardivel A, Bodmer JL, Gaide O, Hertig S, et al. Interactions of tumor necrosis factor (TNF) and TNF receptor family members in the mouse and human. *J Biol Chem*. 2006;281:13964–71.
73. Vince JE, Wong WW, Khan N, Feltham R, Chau D, Ahmed AU, et al. IAP antagonists target cIAP1 to induce TNFalpha-dependent apoptosis. *Cell*. 2007;131:682–93.

ACKNOWLEDGEMENTS

We thank the following people for their technical assistance with the experiments completed in this manuscript; Aira Nuguid and Tina Cardamone (Phenomics Australia Histopathology and Slide Scanning Service - The University of Melbourne), WEHI Bioservices, WEHI Histology Center and WEHI Cytometry Facility. The generation of the *Ripk3*^{-/-} mice used in this study was supported by Phenomics Australia and the Australian Government through the National Collaborative Research Infrastructure Strategy (NCRIS) program. We thank Cynthia Louis and Najoua Lalaoui for the provision of important resources, and Kate Lawlor for helpful discussions.

AUTHOR CONTRIBUTIONS

Conceptualization: ECTC, SEG, JMM, JMH. Methodology: ECTC, SEG, JD, HA, SC, CH, KMP, PG, KRM, ALS. Resources: AH, AJK, IPK, JS, UN, JMM, JMH. Statistical oversight: CSL, ALG. Supervision: IPW, JS, ALS, JMM, JMH. Funding acquisition: IPW, JS, JMM, JMH. Writing: ECTC, SEG, JMM and JMH co-wrote the paper with input from authors.

FUNDING

We are grateful to the National Health and Medical Research Council for fellowship (IPW, 1154325; JS, 1195038; JMM, 1172929; JMH, 1142669), grant (IPW, 1113577; ALS, 2002965; JMH, 2011584) and infrastructure (IRIIS 9000719) support; Anaxis Pharma Pty Ltd for funding support; and the Victorian State Government Operational Infrastructure Support scheme. JD is supported by project grants from the Sylvia and Charles Viertel Charitable Foundation and Royal Australian College of Physicians. KRM was supported by an Arthritis Australia project grant. JD and IPW gratefully acknowledge the support of the Reid Charitable Trusts. We also acknowledge scholarship support for SEG (Australian Government Research Training Program Stipend Scholarship, Wendy Dowsett Scholarship), SC (WEHI Handman PhD Scholarship) and ECTC (Attracting and Retaining Clinician-Scientists' Scholarship). Open Access funding enabled and organized by CAUL and its Member Institutions.

COMPETING INTERESTS

SEG, AH, KMP, PG, IPW, JS, UN, ALS, JMM and JMH contribute to or have contributed to a project developing necroptosis inhibitors in collaboration with Anaxis Pharma. The other authors declare no competing interests.

ETHICS

All experiments were approved by the WEHI Animal Ethics Committee following the Prevention of Cruelty to Animals Act (1996) and the Australian National Health and Medical Research Council Code of Practice for the Care and Use of Animals for Scientific Purposes (1997).

ADDITIONAL INFORMATION

Supplementary information The online version contains supplementary material available at <https://doi.org/10.1038/s41418-023-01121-4>.

Correspondence and requests for materials should be addressed to James M. Murphy or Joanne M. Hildebrand.

Reprints and permission information is available at <http://www.nature.com/reprints>

Publisher's note Springer Nature remains neutral with regard to jurisdictional claims in published maps and institutional affiliations.



Open Access This article is licensed under a Creative Commons Attribution 4.0 International License, which permits use, sharing, adaptation, distribution and reproduction in any medium or format, as long as you give appropriate credit to the original author(s) and the source, provide a link to the Creative Commons license, and indicate if changes were made. The images or other third party material in this article are included in the article's Creative Commons license, unless indicated otherwise in a credit line to the material. If material is not included in the article's Creative Commons license and your intended use is not permitted by statutory regulation or exceeds the permitted use, you will need to obtain permission directly from the copyright holder. To view a copy of this license, visit <http://creativecommons.org/licenses/by/4.0/>.

© The Author(s) 2023, corrected publication 2023